



# Numerical Study on Stress Relief and Fracture Distribution Law of Floor in Short-Distance Coal Seams Mining: A Case Study

Chunlei Zhang · Ruimin Feng · Xibin Zhang · Wei Shen

Received: 12 May 2020 / Accepted: 3 August 2020 / Published online: 19 August 2020  
© Springer Nature Switzerland AG 2020

**Abstract** During the mining process of short distance coal seams group with high gas content, excavation of the protective coal seam will result in stress relief and fracture development which provides pathways for gas migration. Gas stored in the lower coal seam moves along the mining-induced fracture to the floor of the upper working face, which may cause the gas over-limit at the upper coal seam. This paper takes the short distance coal seams group in Xinghua coal mine as an example, theoretical analysis, numerical simulation and field monitoring are

comprehensively applied to study the floor failure mechanism, pressure relief law and dynamic evolution of cracks induced by the mining of the second-right working face. The results showed that as the upper coal seam gradually advances, the pressure relief angle of roof and floor gradually decreases, and the pressure relief range and floor failure depth gradually increase. After the working face of the upper coal seam is advanced 100 m, the range of the pressure relief in the surrounding coal and rock masses approaches stable; the cracks in the shallow depth are mainly with small angles or type II shear cracks, and the cracks in the large depth are mainly shear-expansion with larger angles, and the amount of fractures in the floor reduces with the increase of the depth of the floor. It was found that the mining-induced fractures in the floor is distributed in the shape of an “O” ring, and as the working face advances, the range of this “O”-shaped crack circle keeps moving forward but the width of the crack circle is basically unchanged. Finally, the low-level drilling field was used to control the gas from lower coal seams according to the stress relief and fracture distribution law, which achieved satisfied application effect and provided guidance for mine gas extraction in similar mining conditions.

---

C. Zhang (✉) · W. Shen  
Faculty of Architecture and Civil Engineering, Huaiyin  
Institute of Technology, Huai'an 223001,  
Jiangsu, China  
e-mail: leizhewudi@hyit.edu.cn

C. Zhang  
Department of Mining and Mineral Resources  
Engineering, Southern Illinois University, Carbondale,  
IL 62901, USA

C. Zhang  
School of Mechanics and Civil Engineering, China  
University of Mining and Technology (Beijing),  
Beijing 100083, China

R. Feng  
Department of Chemical and Petroleum Engineering,  
University of Calgary, Calgary T2N 1N4, Canada

X. Zhang  
Huaneng Coal Industry Co., Ltd., Beijing 100070, China

**Keywords** Stress relief · Fracture distribution ·  
Short-distance coal seams · Numerical simulation

## 1 Introduction

Approximately 92% of coal production in China is from underground mining, with an average mining depth of more than 600 m, and the mining depth is still extending downward at a rate of 30–50 m per year (Li et al. 2014; Kong et al. 2019). The underground coal seam occurrence and mining conditions are complicated, and the gas content is generally high. With the increase of the mining depth, the in situ stress, gas pressure and gas content increase significantly, and the possibility of mining being threatened by dynamic disasters such as coal and gas outburst increases, becoming an urgent issue to solve in the deep coal seam mining (Li et al. 2014; Yang et al. 2011; Zhang 2017). Aiming at the problems of low coal seam permeability, poor drainage effect, and coal and gas outburst in China, theoretical research and mining practice showed that the pressure relief mining on protective layers and three-dimensional gas drainage technology can effectively prevent coal and gas outburst (Zhang 2017; Wang et al. 2017). The protective layer mining is capable of changing the stress state and gas dynamic state of the adjacent coal seams, and reducing the pressure of the protected coal seams (Noack 1998; Díaz and González 2007). It is beneficial for the gas flow and desorption of protected coal seam, thereby achieving the purpose of alleviating or preventing coal and gas outburst.

To the best of our knowledge, the mining-induced redistribution of the stress field leads to the initiation and growth of pre-existing cracks, and potentially creates a fractured zone with high conductivity around the excavations (Zhang and Zhang 2016; Lu and Wang 2015). This fractured zone provides pathways for gas and confined water migration, which reduces the effective stresses by increasing the pore pressure in rock strata and in turn further promotes the fracture development (Levasseur et al. 2010; Zhu and Bruhns 2008). During the excavation of short-distance coal seams group with high gas content, and the gas in the lower coal seam moves along the mining-induced fractures in the floor to the upper working face, which will cause the gas over-limit at upper corner. Hence, both gas from protective and protected coal seams must be treated simultaneously. It is necessary to lay out drillings in these regions to stop the methane from flowing into the coal face (Flores 1998). Therefore, it is of great significance to study the pressure relief and

fracture evolution law of the surrounding rock mass during the mining of high gas-content coal seams, for the accurate layout of gas drainage drilling sites and the improvement of gas drainage efficiency.

A lot of research has been conducted on pressure relief and fracture evolution law regarding surrounding rock. Numerical simulation is an effective method for addressing the gas and fracture issues in coal mines but specific features should be considered (Lu and Wang 2015). For a better understanding of pressure relief and fracture development processes, numerous numerical simulations on pressure relief and fracture development during mining processes have been performed with different numerical methods, such as FLAC3D, UDEC, 3DEC, and RFPA (Li 2003). For example, Zhang et al. (2018) established two FLAC3D models with dynamic gob loading characteristics to analyze the effect of gob behavior in the protective coal seam layer on stress relief in the protected coal seam. Li et al. (2018) studied the crack propagation mechanisms and stress evolution of the floor under dynamic disturbance in deep coal mining through 3DEC simulation models, and found that the stress in the bottom effect zone increases nonlinearly with the increasing dynamic disturbance intensity. Zhu et al. (2013) presented a coupled process-based numerical model for mining excavation to analyze the in situ pore pressure change. RFPA is a numerical testing tool for realistic failure process analysis of rock, concrete, composites, and engineering structures. Li et al. (2012) have conducted various RFPA numerical simulations to study the opening-mode fracture initiation and propagation perpendicular to the bedding planes in sedimentary rocks.

Physical simulation is another method widely used to investigate stress distribution and fracture evolution during the excavation of coal seam. Cheng et al. (2016) found that the evolution characteristics of the superimposed mining-induced stress-fissure field were different from the ones of the single coal seam mining by physical models. Li et al. (2016) studied the influence of the monolayer mining and repeated mining on overlying strata movement, fracture distribution and evolution laws, characteristics of abutment pressure distribution and mining-induced fissure elliptic paraboloid zone through physical similarity simulation experiments and theoretical analysis.

Field measurements have also been found to be relatively effective in solving mining-induced

problems, such as the borehole strain method, the borehole ultrasonic imaging method, and the CT electronic imaging method (Hu et al. 2019). Liu et al. (2009) detected the evolution of water conducting fractures in coal seam floors by applying 3D electrical resistivity, which is a method capable of presenting the failure mode of coal seam floor in mining process. Zhang and Liu (2004) applied the CT technique of seismic wave to detect the overburden failure dynamically with face advance. Peng et al. (2010) used the borehole camera method to study the mining-induced fracture field under high strength mining conditions, and discussed the relationship of gas pressure with mining-induced fracture distribution. The disadvantage of field monitoring methods is that these require a large amount of site investment and complex construction processes and cannot be used to generate effective predictive data before mining.

However, most of the previous studies are focused on the coal seam roof, and few studies have been conducted on the floor. It is still required to conduct research on the mining pressure relief range and crack distribution of the coal seam roof and floor under specific engineering geological conditions. Taking a specific coal mine in China as an example, this paper aims at addressing the issue of large gas emission during the mining of high gas coal seams in the second-right working face of #28 coal seam in Xinghua Coal Mine. A combined method of theoretical calculations, numerical simulations and field measurement are used to analyze the pressure relief rules and fracture evolution law of the coal seam floor during the excavation of the upper protective coal seam. The research results will provide a basis for the gas drainage design, and solve the issues regarding gas concentration for Xinghua coal mine, which provides a guidance in gas control for the coal mines with similar mining or geological conditions.

## 2 Engineering Background

The case working face is located in #28 coal seam, which is in the second panel of the west part. It has a strike length of 560 m and an inclined length of 200 m. The average thickness of the coal seam is 1.2 m and its inclination angle is  $2^\circ$ . #27 coal seam is approximately 0.5 m above the #28 coal seam. As shown in Fig. 1, 6–8 m and 22 m below #28 coal seam

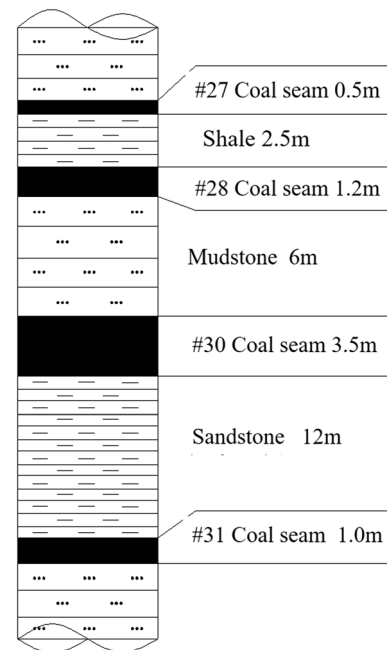


**Fig. 1** Stratigraphic column of Xinghua coal mine

are #30 and #31 coal seam, respectively. The absolute and relative gas emission rate in the working face area is  $70 \text{ m}^3/\text{min}$  and  $51 \text{ m}^3/\text{t}$ . Field observation indicated that during the excavation of #28 coal seam, the absolute gas emission rate of this layer and the upper #27 coal seam is  $30\text{--}40 \text{ m}^3/\text{min}$ , and the gas emission of the lower #30 and #31 coal seam is about  $40 \text{ m}^3/\text{min}$ . Due to the large amount of gas emission from the working face, a special gas gateway was driven. When mining the second-right working face of the layer #28, the high-level drainage tailings and high-level drilling fields reserved in goaf can only effectively drain the gas in the gob of this coal seam. For the overflow gas from the coal seams below #28 coal seam, enhanced gas drainage measures must be adopted to reduce the gas content. Therefore, it is necessary to determine the mining pressure relief range and gas accumulation law of the floor, and then provide a design basis for the gas drainage project.

## 3 Theoretical Analysis of the Floor Failure Depth

During the mining of coal seams group, the mining of adjacent coal seams will affect each other, especially when the distance between two coal seams is close, the

roof of the lower coal seam will be affected by the mining of the upper coal seam to different degrees of damage and destruction (Peng et al. 2019). Therefore, the overburden migration and mining-induced stress redistribution caused by the mining of lower coal seams are different from those of single coal seam mining. In the appendix of China's "Safety Regulation for Coal Mining" (2016), the short-distance coal seams are interpreted as "coal seams that are close and have a great influence on each other during mining." Literature (Zhang et al. 2005) states that when  $h_f$  (distance between two coal seams) satisfies  $h_f \leq h$  (floor failure depth after excavation), the coal seam group is a close-range coal seam group.

In the case study coal mine, #28 coal seam was excavated firstly, then its influence area below it was studied. According to the Mohr–Coulomb failure criterion, the maximum failure depth ( $h_{\max}$ ) of the floor is determined by the following formula (Zhang 2008):

$$h_{\max} = \frac{1.57\gamma^2 H^2 L_x}{4\beta^2 \sigma_c^2} \quad (1)$$

The maximum floor depth ( $h_{\max}$ ) can also be obtained by the empirical prediction formula (Wang et al. 2010):

$$h_{\max 2} = 0.0113H + 6.25 \ln(L_x/40) + 2.52 \ln(M/1.48) \quad (2)$$

where  $L_x$  is the working face width,  $\sigma_c$  is the average uniaxial compressive strength of the floor,  $H$  is the average mining depth,  $\gamma$  is the average bulk density,  $\beta$  is the influence coefficient of rock mass joints, and  $M$  is the mining height. According to the mining condition of the case coal mine, the parameters obtained for the case mine are given as:  $L_x = 200$  m,  $\sigma_c = 60$  Mpa,  $H = 620$  m,  $\beta = 0.7$ , and  $M = 1.2$  m.

From Eq (1), it can be seen that the floor failure depth is positively proportional to the mining depth and the working face width. By substituting the parameters into Eqs. (1) and (2), the maximum failure depth of the floor is 10.60 and 16.48 m, respectively, which exceed the distance between #28 coal seam and #30 coal seam. It indicates that the excavation of #28 coal seam caused damage to the #28 coal seam floor and #30 coal seam.

## 4 Stress and Displacement Distribution in Coal Seam Floors

### 4.1 FLAC 3D Modeling

In this paper, FLAC3D modeling was firstly used to investigate the stress and displacement distribution around the excavation of #28 coal seam, especially in the floor. The size of the model is 400 m (X) × 500 m (Y) × 120 m (Z), A free top boundary is adopted by the model but 7.5 MPa vertical stress is applied on the top to represent the overburden, and meanwhile all displacements on the bottom and the horizontal directions are restricted. As shown in Fig. 2, the working face advances in the X direction (from left to the right). The face width and length in the model is 100 and 200 m, respectively. Mohr–Coulomb mechanical criterion is applied in the model and the rock mechanics parameters used are listed in Table 1.

With the advancement of the working face, the stress in the roof and floor of the #28 coal seam was redistributed. From Fig. 2a, it can be seen that the stress reduction zone appears on the roof and floor when the working face is advanced 30 m. Taking the stress variation coefficient  $k = 0.4$  as the pressure relief boundary (Zhang et al. 2018), the definition of pressure relief angle can be referred to Zhang et al. (2018), the pressure relief angle of the roof is  $72^\circ$  and the pressure relief height is 20 m. The pressure relief angle of the floor is  $69^\circ$  and the pressure depth is 20 m. It has had a great impact on the lower 30# coal seam. As shown in Fig. 2b–d, with the further advance of the working face, the range of stress reduction zones of surrounding rock mass gradually expands, the pressure relief angle gradually decreases, and the pressure relief depth increases. When the working face is advanced to 60 m, the pressure relief angle of the roof is  $68^\circ$ , the pressure relief height reaches 26 m, the pressure relief angle of the floor is  $70^\circ$ , and the pressure relief depth has exceeded the floor of 31# coal seam. After driving the working face for 100 m, the mining-induced pressure relief ranges of the surrounding rock masses have generally stabilized. The pressure relief angles of the roof and floor are  $63^\circ$  and  $67^\circ$ , respectively. And the pressure relief height reaches 31 m. It means that the excavation of #28 coal seam working face can release pressure of the coal seam above and below it.

By analyzing the plastic zone of the surrounding rock mass during the excavation of #28 coal seam, it is

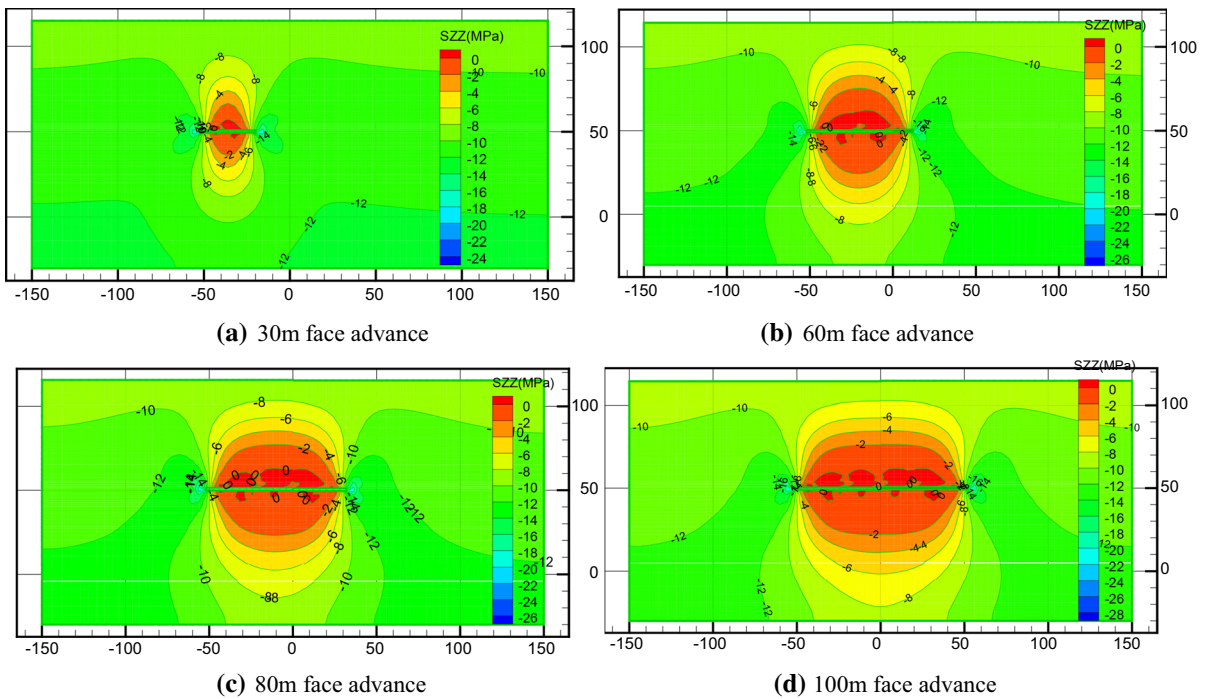


**Fig. 2** The stress distribution of floor for different face advance of #28 coal seam

**Table 1** The coal and rock mechanics parameters used during FLAC 3D modeling

Lithology	Density (kg/m <sup>3</sup> )	Bulk modulus (GPa)	Shear modulus (GPa)	Cohesion (MPa)	Tensile strength (MPa)	Internal friction angle (°)
Medium sandstone	2500	6.2	4.9	10	4.5	42
Fine sandstone	2600	2.5	2.0	5.6	1.2	30
Shale	2560	2.96	1.39	3.2	2.1	29
#28 Coal seam	1350	1.5	0.5	0.6	0.2	20
Mudstone	2200	1.8	1.0	1.2	0.6	18
#30 Coal seam	1350	1.5	0.5	0.6	0.2	20
Sandstone	2200	2.0	1.2	1.4	0.8	19
#31 Coal seam	1350	1.5	0.5	0.6	0.2	20
Fine sandstone	2500	6.5	4.9	12	4.7	43

found that the damage range of the roof and floor increases with the working face advancing. When the working face is advanced 30 m, the plastic deformation height of roof is about 10 m, and the plastic deformation depth of the floor is about 9.5 m. Most of the lower #30 coal seam has been damaged due to shear failure; when the coal seam is excavated for 60 m, the plastic deformation height of the roof has

reached 17.5 m and the tensile failure is the dominated failure mode. Shear failure occurs in the immediate floor of the #30 coal seam, while partial damage occurs in the lower #31 coal seam. This is because the strength of the coal is small and the shear deformation occurs under the influence of the mining-induced stress. When the working face advances to 100 m, the roof plastic deformation height is about 22.5 m, and

the floor plastic deformation depth is still about 11.5 m (as shown in Fig. 3). And shear plastic deformation has occurred in most part of #31 coal seam. When the working face continues to advance, the plastic deformation depth of the roof and floor no longer increase.

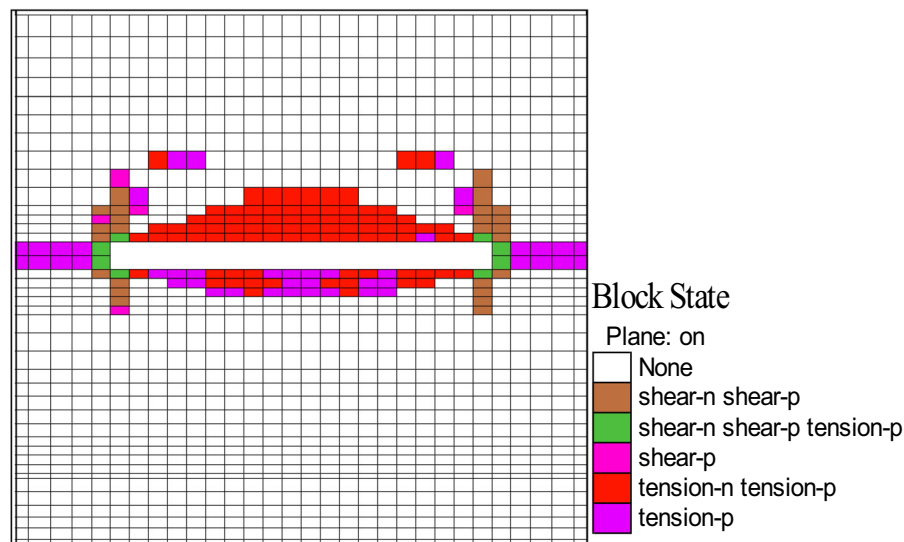
#### 4.2 Pressure Relief Characteristics

Figure 4 shows the displacement and stress variation of #30 coal seam in the central of #28 coal seam gob floor after 100 m face advance of #28 coal seam. From the monitoring results of the vertical displacement of the #30 coal seam, it can be seen that when the working face advances to the middle position of the model, the displacement and vertical stress of the #30 coal seam get increased. When the model runs to 1570 time steps, the vertical compression displacement of #30 coal seam at the  $x = 0$  position in the middle of the gob reaches a maximum of  $-7.3$  cm; when running to 1830 time steps, the vertical stress of the 30# coal seam at the  $x = 0$  position reaches the maximum value of  $-13$  Mpa; and then the displacement and stress of the coal seam decrease rapidly with the time step increasing. After running 2600 time steps, the vertical displacement stabilizes at  $-2.5$  cm and the vertical stress stabilizes at  $-0.1$  Mpa (Fig. 4).

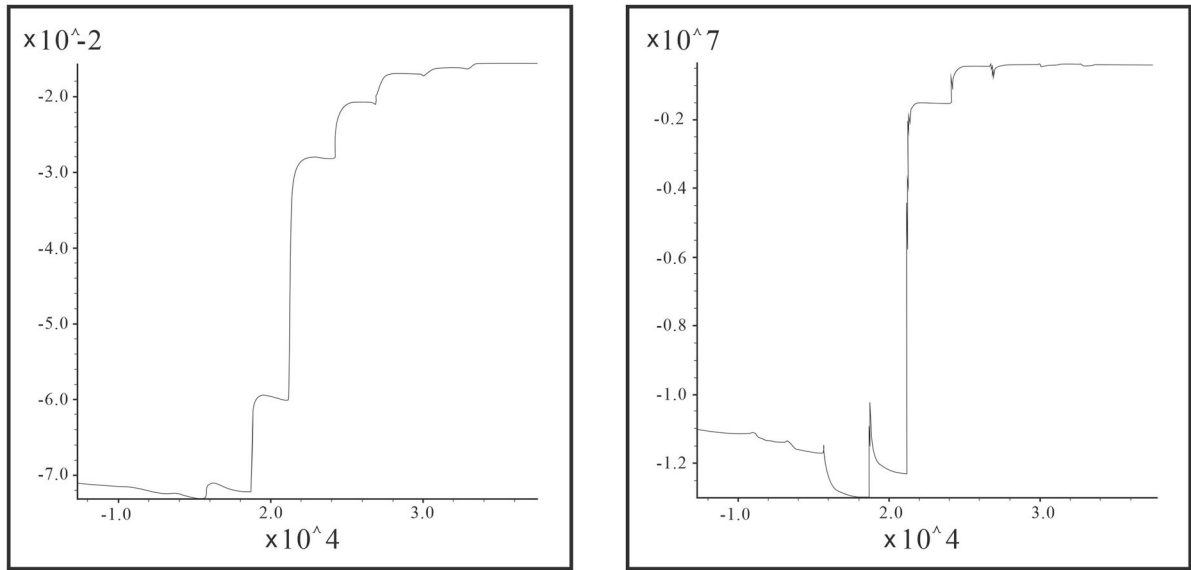
As shown in Fig. 5, from the stress distribution of the #30 coal seam floor after 120 m face advance, it can be known that the peak value of the vertical stress

of the #30 coal seam is about 12 m ahead of the working face, and the stress concentration factor is 1.7. The vertical stress decreases to the minimum value 5 MPa at 12 m behind the working face, and then basically stabilized at this stress to the back of the goaf. The stress  $\sigma_{yy}$  value along the inclination of the working face does not change much, and its change trend is basically the same as the vertical stress, but its stable value is greater than the vertical stress. The change trend of the stress  $\sigma_{xx}$  along the advancing direction of the working face is different from the vertical stress, reaching a minimum value of about 2 MPa at about 4 m in front of the working face (8 m behind the peak of vertical stress), and the stress increases to 3 MPa at 4 m behind the coal face, and then stabilized at about 0.2 MPa. The change law of stress  $\sigma_{xx}$  reflects the deformation and flow process of the coal seam in the floor to the gob side under the influence of vertical stress.

Figure 6 shows the displacement distribution of #30 coal seam after 120 m face advance of #28 coal seam. It can be seen from Fig. 6 that the vertical displacement distribution of #30 coal seam is consistent with its vertical stress distribution. The vertical displacement reaches its maximum at about 14 m ahead of the working face, which is about  $-5.7$  cm, the vertical displacement continued to decrease toward the goaf, and the minimum displacement is about 1 mm at about 28 m behind the coal face. The



**Fig. 3** Plastic zone distribution for 100 m face advance



(a) Vertical displacement change of point  $x=0, y=0, z=42$

(b) Vertical stress change of point  $x=0, y=0, z=42$

**Fig. 4** Displacement, stress change of #30 coal seam in the central of #28 coal seam gob floor after 100 m face advance of # 28 coal seam

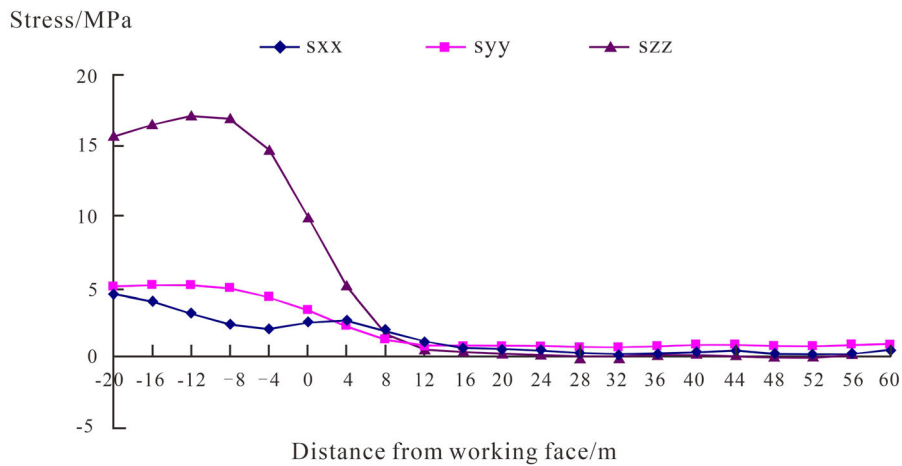


**Fig. 5** Stress distribution of #30 coal seam after 120 m face advance of #28 coal seam

displacement of y-dis along the inclined direction of the working face remains unchanged; the displacement x-dis along the working face advancing direction begins to decrease from 16 m in front of the working face. It becomes positive at 4 m behind the working face, which indicates that the coal seam is deformed to the side of the goaf, but it becomes negative again under the pressure of the collapsed rock mass at about 24 m behind the coal face.

### 5 Fracture Evolution Law of Coal and Rock Mass in the Floor

Based on the theoretical characteristics of discrete element method, UDEC software can simulate the discontinuous medium of coal and rock mass with joints and fractures. It can reflect the distribution rules of fractures through the movement and failure of surrounding rock under the influence of mining and achieve a better effect on the evolution regularity of

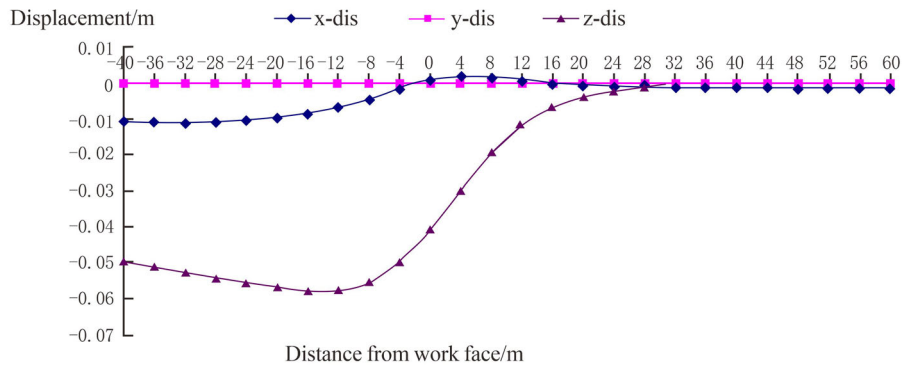


**Fig. 6** Displacement distribution of #30 coal seam after 120 m face advance of #28 coal seam

surrounding rock fractures under the influence of coal mining (Zhang 2017). So UDEC numerical simulation software was used to simulate the fracture development characteristics of floor rock mass and #30 coal seam during the excavation of #28 coal seam. The simulation assumes that there are pre-existing fissures distributed in all directions of the coal seam, and establishes random joints in the lower coal seam (in the floor of #28 coal seam) of model. However, due to the high strength of the floor rock layer, the crack direction in which the expansion occurs is the same as the principal stress direction, and it is mainly distributed vertically and horizontally. Hence, only the vertical and horizontal joints are established in the model.

After the excavation of #28 coal seam, the stress of the coal and rock mass in the floor will be redistributed. As is shown in Fig. 7, due to the advanced abutment pressure of the working face, a certain range of the coal and rock mass of the floor in front of the working face is in the compression zone, and the coal

rock mass in this area is affected by the vertical stress. The main failure modes are compression and shear failure. The pre-existing fractures and cracks are often compacted. The permeability of the surrounding rock mass is reduced under compression, but under the mining-induced high stress, tensile extension cracks in the direction of the principal stresses initialize and expand. From the peak value of the vertical stress in front of the working face to the vertical stress reduced to the level of confining pressure behind the mined-out area is the transition zone of the floor. In this range, the vertical stress is continuously reduced while the confining pressure remains relatively stable. It can be regarded as an unloading process of the vertical stress. Expansion cracks is dominated by sliding in this range. From the vertical stress reduced to the level of confining pressure behind the coal face to the edge of compaction zone in gob is in decompression area. This area can be regarded as the decompression zone. The coal and rock mass in this zone changes from a high stress area to a low stress area, and the state changes

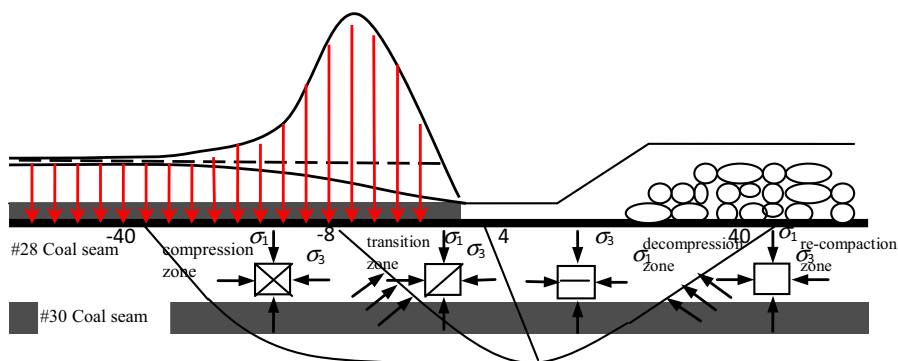


**Fig. 7** Mechanical characteristics and division of floor coal and rock (Zhang et al. 2015)



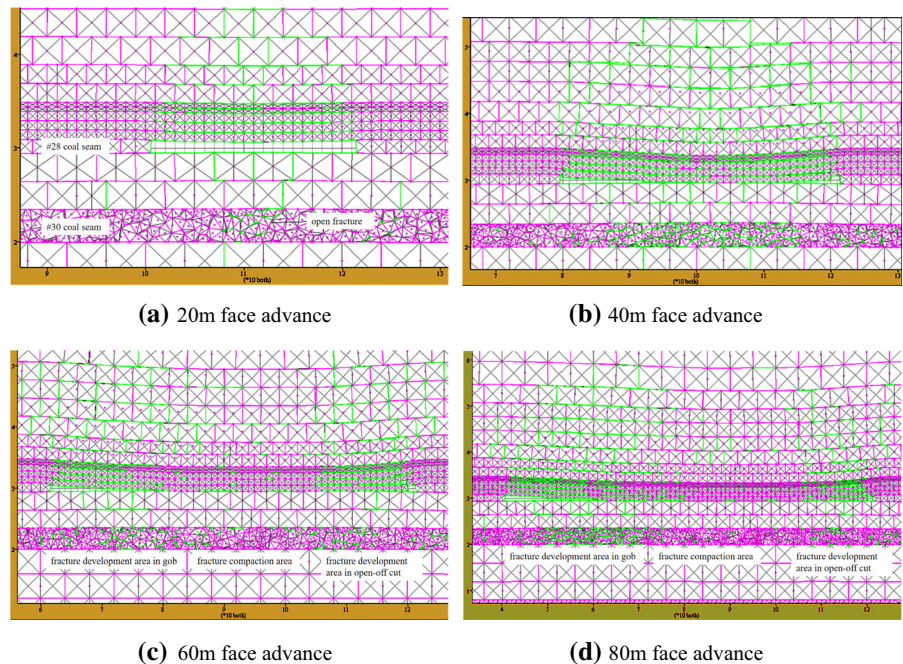
from a compressed state to an expanded state. Tensile failure will occur, and then result in floor heave. The bedding fracture along the rock layer and vertical penetration cracks will be generated, increasing the permeability coefficient of surrounding rock mass. In the back of the decompression zone is the re-compaction zone. The collapsed strata in the compacted area behind the goaf are compacted by overlying strata, leading to the increased vertical stress in coal and rock mass of the floor within this range. The rock mass changes from the expanded state to the compacted state, and the open cracks are compacted again.

Figure 8 shows cracks development characteristics of the floor coal and rock mass. From the simulation results, it can be seen that when the working face advances 20 m, the coal and rock mass in the gob area undergoes expansion deformation. Tensile cracks develop in floor coal in the middle of the goaf area, and the crack development angle is mostly horizontal or slightly inclined. Penetrating vertical cracks are mainly developed in interval layers. The first roof caving occurs when the working face advances 40 m, and the coal fractures in the middle of the mined-out area continue to develop, the fracture extension range increases, and the bedding layer open cracks appear in the interval rock layer. When the working face

advances for 60 m, the collapse of the roof in the mined-out area compacts and the open crack in the middle of floor is closed. The fissure development area exists only behind the coal wall and near the open-off cut area. At this time, the development characteristics of the coal seam in the goaf are roughly divided into three areas: the fractured zone, from the face to 30 m back of the goaf; the compacted zone, about 15 m in the middle of the goaf; and the fissure development area, about 20 m near the open-off cut. After 80 m face advance, the fissure development area of the floor moves forward with the advancement of the working face, but the width of the fissure development area remains basically stable, and the scope of the crack compaction area in the middle of the goaf is expanded. The area of the fissure development area near the open-off cut side is basically unchanged. It can be seen that the development zone of mining-induced pressure relief fractures in the floor is also distributed in an “O” circle shape. The width of this “O” circle near the coal face is about 30 m, and the width in the open-off cut area is about 20 m, the range of this “O” circle moves forward as the working face advances while the width of the crack circle is basically unchanged, as shown in Fig. 8.

After 80 m face advance, the Cracks’ angle distributions in different depth of floor is shown in Table 2.

**Fig. 8** Cracks development characteristic of floor coal and rock mass during coal seam excavation



It is known that there are 37 cracks at a depth of 0–2 m, and a total of 14 cracks with an inclination angle less than or equal to 30° account for 37.84%. A total of 5 cracks of 31°–45° account for 13.51%, a total of 5 cracks of 46°–60° account for 13.51%, a total of 6 cracks of 61°–75° account for 16.22%, and there are 7 cracks with an inclination of 76°–90°, accounting for 18.92%. Cracks with an inclination angle of less than 45° account for 51.35%, which is more than half total cracks.

A total of 40 cracks were obtained from the depth of 2–4 m. Among them, 17 cracks with an inclination angle less or equal to 30° account for 42.5%, and 7 cracks with an inclination angle of 31°–45° account for 17.50%, a total of 5 cracks with an inclination angle of 46°–60° account for 12.50%, a total of 4 cracks with an inclination angle of 61°–75° account for 10.00%, and a total of 7 cracks with an inclination angle of 76°–90° account for 17.50%. Cracks with an inclination angle of less than 45° account for 60.0%, which is more than half of total cracks.

A total of 20 cracks were obtained from the depth of 4–6 m. Among them, 9 cracks with an inclination angle less or equal to 30° account for 45%, and 2 cracks with an inclination angle of 31°–45° account for 10%, a total of 2 cracks with an inclination angle of 46°–60° account for 10%, a total of 2 cracks with an inclination angle of 61°–75° account for 10%, and a total of 2 cracks with an inclination angle of 76°–90° account for 10%. Cracks with an inclination angle of less than 45° account for 55%, which is more than half of total cracks.

A total of 10 cracks were obtained from the depth of 6–8 m. Among them, 3 cracks with an inclination angle less or equal to 30° account for 30%, and 1 cracks with an inclination angle of 31°–45° account

for 10%, a total of 1 cracks with an inclination angle of 46°–60° account for 10%, a total of 5 cracks with an inclination angle of 61°–75° account for 50%, and there is no crack with an inclination angle of 76°–90°. Cracks with an inclination angle of more than 45° is more than half of total cracks.

A total of 5 cracks were obtained from the depth of 8–10 m. Among them, there is no crack with an inclination angle less or equal to 30°, and 1 cracks with an inclination angle of 31°–45° account for 20%, a total of 2 cracks with an inclination angle of 46°–60° account for 40%, only 1 crack with an inclination angle of 61°–75° account for 20%, and the number of crack with an inclination angle of 76°–90° is also 1. Cracks with an inclination angle of more than 45° is more than half of total cracks.

It can be seen from the distribution characteristics of the floor fissures after 80 m face advance that the number of cracks gradually decreases with the increase of the floor depth until it no longer develops (Fig. 9). In the shallow part of the floor, tensile cracks or mode II shear cracks with a small inclination angle are dominant, while in the deep part, compression-shear cracks with a large inclination angle are dominant. This is consistent with the mechanism analysis of crack propagation in coal and rock mass. The horizontal deformation of the coal and rock mass in the deep part of the floor is restricted by the surrounding rock, and the crack propagation direction is the same as the principal stress direction while in the shallow part, the vertical stress decreases and the restrict from horizontal surrounding rock weakens, and the crack propagation is mainly expansion and shear mode.

**Table 2** Cracks' angle distributions in different depth of floor

Angle	Depth									
	0–2 m		2–4 m		4–6 m		6–8 m		8–10 m	
	Qty	%	Qty	%	Qty	%	Qty	%	Qty	%
≤ 30°	14	37.84	17	42.5	9	45	3	30	0	0
31°–45°	5	13.51	7	17.5	2	10	1	10	1	20
46°–60°	5	13.51	5	12.5	2	10	1	10	2	40
61°–75°	6	16.22	4	10	2	10	5	50	1	20
76°–90°	7	18.92	7	17.5	5	25	0	0	1	20
Total Qty	37		40		20		10		5	

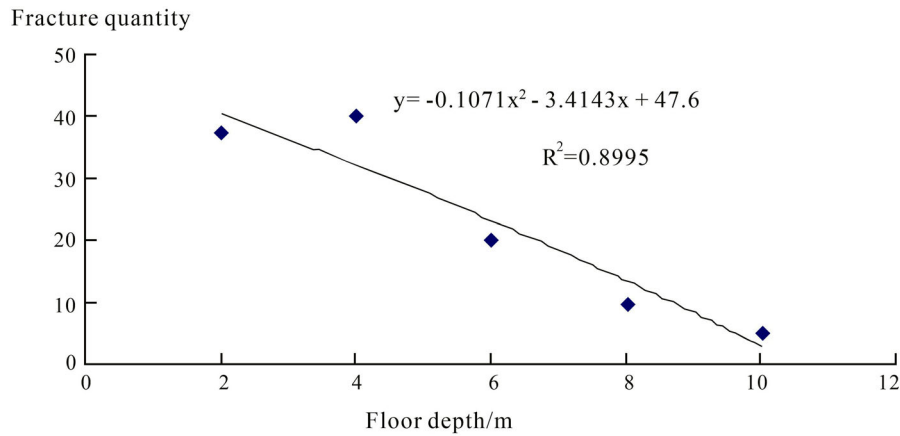


**Fig. 9** The relationship between fracture' quantity and depth of floor after 80 m face advance

**6 Field Measurement**

Through drilling and inspecting the floor coal and rock mass in the field, the development characteristics of the macro-cracks of the coal and rock mass at different depths of floor in the abutment zone of the working face were studied. Floor drillings are arranged at 30, 10, and 5 m in front of the second-right working face of the 28# coal seam in Xinghua Coal Mine. The drilling depths are 4.5, 2.5, and 1.8 m. The TYGD10 rock formation drilling detector was used to detect the drilling of the floor (Peng et al. 2010). The crack development, deformation and failure characteristics of the floor coal and rock mass at different positions

and depths in front of the working face were obtained (Figs. 10, 11, 12).

The results in Figs. 10, 11 and 12 show that as the distance from the working face decreases, the degree of damage to the floor coal and rock mass continues to increase. There are fewer cracks in the floor at 30 m in front of the working face, but the cracks can be clearly observed in the 10 m drilling hole in front of the working face. The floor coal and rock mass at 5 m in front of the working face becomes broken. It is shown that with the decrease of distance from the coal face, the floor coal and rock mass has undergone the processes of compressive and tensile crack growth, reverse slip crack growth, and expansion shear crack

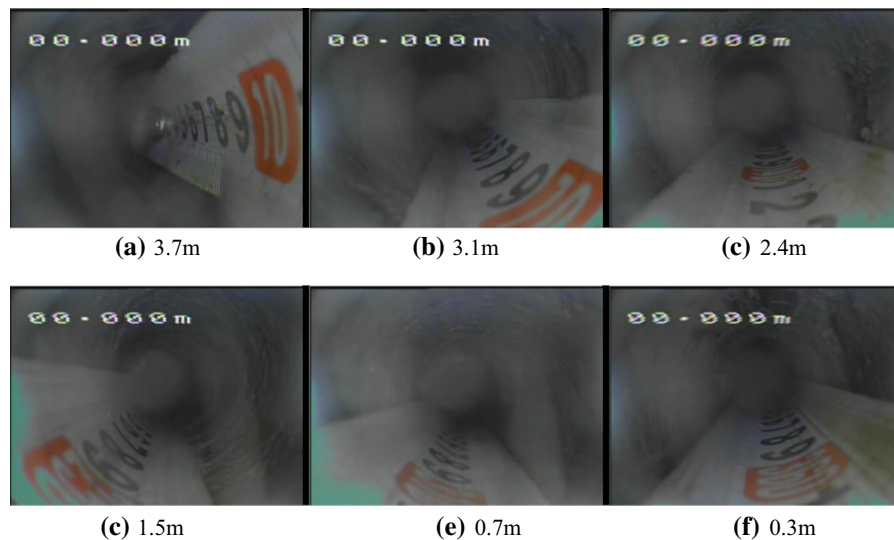


**Fig. 10** Imaging of the floor borehole at 30 m ahead of the face

**Fig. 11** Imaging of the floor borehole at 10 m ahead of the face

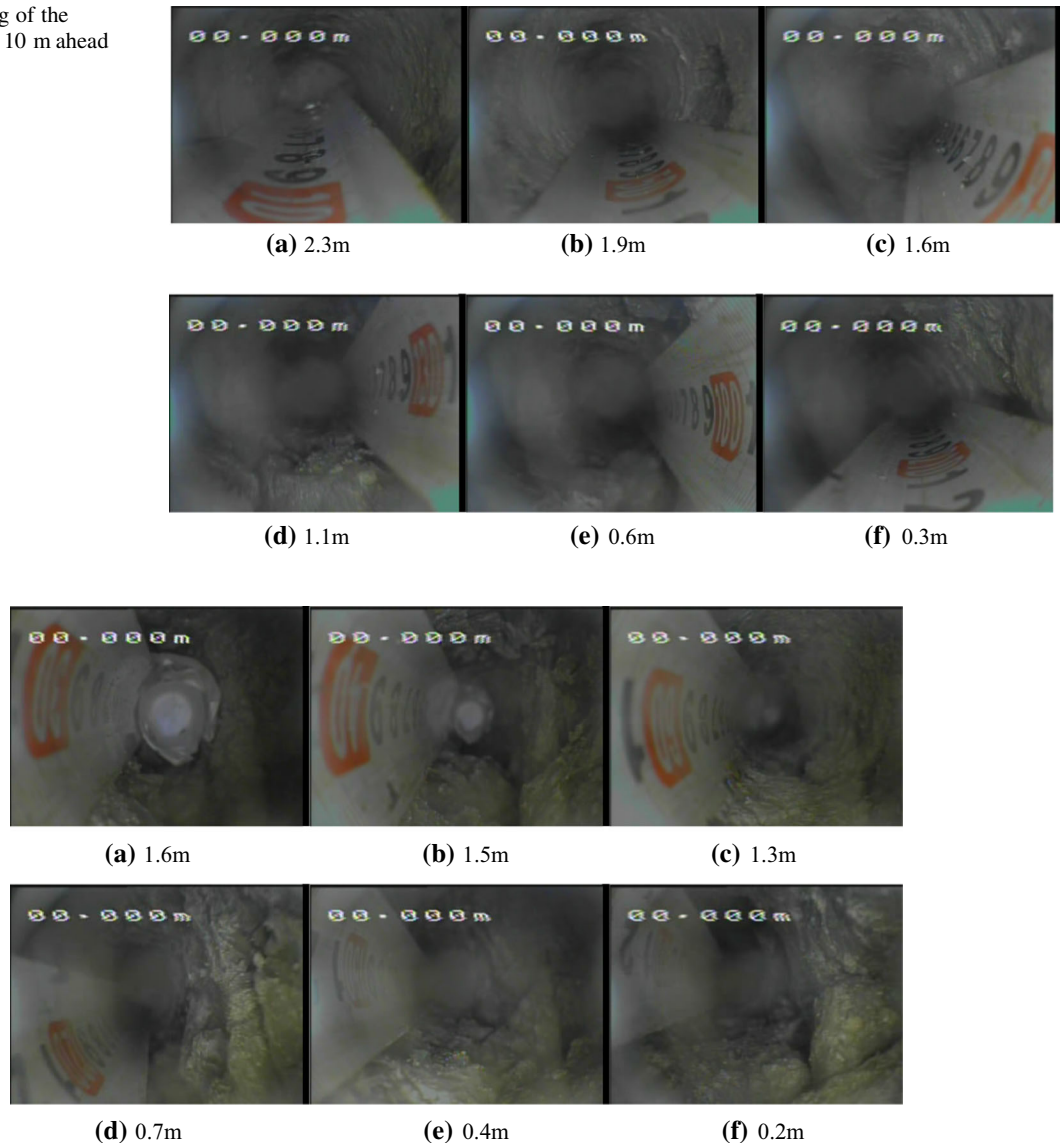


**Fig. 12** Imaging of the floor borehole at 5 m ahead the face

growth. The cracks continue to develop and the coal and rock mass damage is intensified. Cracks development in the shallow part of the floor is more serious than those in the deep part of the floor. The vertical cracks are dominated in the deep part of the borehole, while the bedding cracks and comprehensive connected cracks are dominated in the shallow part of the borehole. The field monitoring results are completely in agreement with the numerical simulation results, which verifies the crack propagation mechanism obtained from the simulation.

## 7 Gas Drainage Scheme

In order to solve the problem of gas over-limit caused by the gas overflow from the floor to the working face, a sloped lane in the intake airflow roadway was constructed from the floor of the second-right working face in #28 coal seam to the roof of #30 coal seam which is 200 m ahead of the coal face, then a 15 m long and 5 m wide drilling site along the #30 coal seam roof was built for drainage of gas released from #30 coal seam and #31 coal seam (Fig. 13). 16

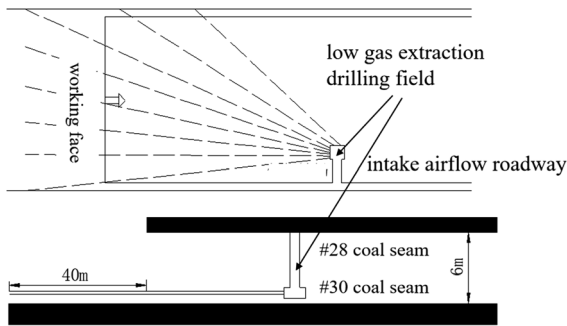


**Fig. 13** Low gas extraction drilling field

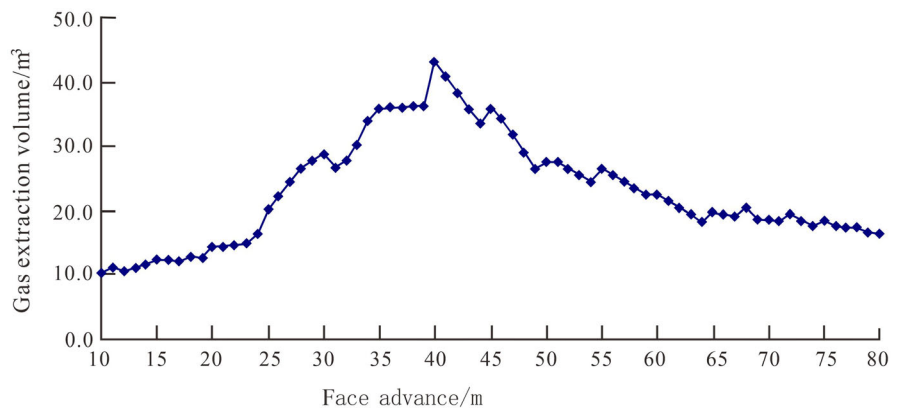
horizontal boreholes were arranged in the drilling field, with a length of 260–300 m for each borehole, and after a spacing of 200 m was the second drilling site. Stubble length of borehole was greater than 40 m. After the project was implemented, the burden of gas discharge on the working face was greatly reduced, gas concentration on the working face and the return airflow roadway was not exceeded, and the production capacity of the working face was improved. The gas extraction volume of the drainage pump reached 43 m<sup>3</sup>/min, and the gas drainage rate reached 54% (as shown in Fig. 14), and the comprehensive treatment effect was effective.

### 8 Conclusions

1. Based on different theoretical calculations, the floor failure depth after the excavation of # 28 coal seam is 10.6 and 16.48 m, respectively, which indicates that the impact range of the mining of the

- # 28 coal seam has included # 30 coal seam and # 31 coal seam;
2. The FLAC3D numerical simulation results show that as the upper coal seam gradually advances, the pressure relief angle of roof and floor gradually decreases, and the pressure relief range gradually increases. After the working face is advanced for 100 m, the range of pressure relief for surrounding coal and rock masses on roof and floor has approximately been stable. And shear failure is the dominant form of coal seam floor. The change law of stress  $S_{xx}$  reflects the deformation and flow process of floor to gob side under the influence of vertical stress.
3. The distribution laws of crack angle at different depths of floor and the relationship between floor depth and fracture number are acquired through UDEC simulation software and field monitoring, the results show that the number of fractures in the floor decreases with the depth of the floor until it is no longer developed. The cracks in the shallow depth are mainly with small angle or II type shear crack, and the cracks in the large depth are mainly shear-expansion with lager angle. The mining-induced fractures in the floor is distributed in the shape of an “O” ring. As the working face advances, the range of this “O”-shape crack circle keeps moving forward but the width of the crack circle is basically unchanged.
4. Based on the analysis of floor failure regularity, pressure relief laws, and field practical experience, the low-drilling field were set up for the gas control of 30 # and 31 # coal seam. Good gas management results were achieved.

**Fig. 14** Extraction effect of discharging pressure coal seam gas



**Acknowledgements** This paper was supported by the State Key Research Development Program of China (Grant No. 2016YFC0600708), the National Natural Science Foundation of China (51804129, 51808246, 51904112), the Jiangsu Post-doctoral Research Funding Project (2019K139), science and technology projects of Ministry of Housing and Urban–Rural Development of the People’s Republic of China (2017K6004), and the Foundation of Huaiyin Institute of Technology. The authors would also like to express special thanks to the editor and anonymous reviewers for their professional and constructive suggestion.

## References

- Cheng ZH, Qi QX, Li HY et al (2016) Evolution of the super-imposed mining induced stress-fissure field under extracting of close distance coal seam group. *J China Coal Soc* 41(2):367–375 (in Chinese)
- Díaz AMB, González NC (2007) Control and prevention of gas outbursts in coal mines, Riosa-Olloniego coalfield, Spain. *Int J Coal Geol* 69:253–266
- Flores RM (1998) Coalbed methane: from hazard to resource. *Int J Coal Geol* 35:3–26
- Hu YB, Li WP, Wang QQ et al (2019) Study on failure depth of coal seam floor in deep mining. *Environ Earth Sci* 78:697
- Kong DZ, Cheng ZB, Zheng SS (2019) Study on the failure mechanism and stability control measures in a large-cutting-height coal mining face with a deep-buried seam. *B Eng Geol Environ* 78(8):6143–6157
- Levasseur S, Charlier R, Frieg B et al (2010) Hydro-mechanical modelling of the excavation damaged zone around an underground excavation at Mont Terri Rock Laboratory. *Int J Rock Mech Min* 47(3):414–425
- Li J (2003) A review of techniques, advances and outstanding issues in numerical modelling for rock mechanics and rock engineering. *Int J Rock Mech Min* 40(3):283–353
- Li LC, Tang CA, Wang SY (2012) A numerical investigation of fracture infilling and spacing in layered rocks subjected to hydro-mechanical Loading. *Rock Mech Rock Eng* 45:753–765
- Li W, Cheng YP, Guo PK et al (2014) The evolution of permeability and gas composition during remote protective longwall mining and stress-relief gas drainage: a case study of the underground Haishiwan Coal Mine. *Geosci J* 18(4):427–437
- Li SG, Ding Y, An ZF et al (2016) Experimental research on the shape and dynamic evolution of repeated mining-induced fractures in short-distance coal seams. *J Min Safety Eng* 33(5):904–910 (in Chinese)
- Li CY, Zhang Y, Zhang GJ et al (2018) Crack propagation mechanisms and stress evolution of floor under dynamic disturbance in deep coal mining. *Chin J Geotech Eng* 40(11):2031–2040 (in Chinese)
- Liu SC, Liu XM, Jiang ZH et al (2009) Research on electrical prediction for evaluating water conducting fracture zones in coal seam floor. *China J Rock Mech Eng* 28(2):348–356
- Lu YL, Wang LG (2015) Numerical simulation of mining-induced fracture evolution and water flow in coal seam floor above a confined aquifer. *Comput Geotech* 67:157–171
- National Coal Mine Safety Administration (2016) Safety Regulation for Coal Mining. China Coal Industry Publishing House, Beijing (in Chinese)
- Noack K (1998) Control of gas emissions in underground coal mines. *Int J Coal Geol* 35:57–82
- Peng YW, Qi QX, Wang YG et al (2010) Study of field measurement of mining-induced coal fracture field and its application. *Chin J Rock Mech Eng* 29(S2):4188–4193 (in Chinese)
- Peng GY, Gao MZ, Lv YC et al (2019) Investigation on mining mechanics behavior of deep close distance seam group. *J China Coal Soc* 44(7):1971–1980 (in Chinese)
- Wang JC, Xu YC, Xu GM et al (2010) Application of mine electric profiling method to detect floor failure depth of coal mining face. *Coal Sci Technol* 38(1):97–100 (in Chinese)
- Wang FT, Zhang C, Liang NN (2017) Gas permeability evolution mechanism and comprehensive gas drainage technology for thin coal seam mining. *Energies* 10:1382
- Yang W, Lin BQ, Qu YA et al (2011) Mechanism of strata deformation under protective seam and its application for relieved methane control. *Int J Coal Geol* 85(3):300–306
- Zhang BS (2008) Study on the surrounding rock control theory and technology of ultra-close multiple-seams mining. Doctoral Dissertation, Taiyuan University of Technology, Taiyuan, p 27
- Zhang CL (2017) Fracture development and stress relief with space influenced by mining of coal seams group. Doctoral Dissertation, China University of Mining and Technology, Beijing
- Zhang PS, Liu SD (2004) Observation of overburden failure of coal seam by CT of seismic wave. *Chin J Rock Mech Eng* 23(15):2510–2513 (in Chinese)
- Zhang CL, Zhang Y (2016) Stress and fracture evolution based on abutment change in thick coal seam—A case study in china colliery. *Electron J Geotech Eng* 21:4369–4386
- Zhang BS, Kang LX, Zhai YD (2005) Definition of ultra-close multiple-seams and its ground pressure behavior. In: The 24th international conference on ground control in mining, Morgantown, W.V., pp 110–113
- Zhang Y, Zhang CL, Zhao F (2015) Dynamic evolution rules of mining-induced fractures in different floor area of short-distance coal seams. *J China Coal Soc* 40(4):786–792 (in Chinese)
- Zhang CL, Yu L, Feng RM et al (2018) A numerical study of stress distribution and fracture development above a protective coal seam in longwall mining. *Processes* 6(9):146
- Zhu WC, Bruhns OT (2008) Simulating excavation damaged zone around a circular opening under hydromechanical conditions. *Int J Rock Mech Min* 45(5):815–830
- Zhu B, Wu Q, Yang JW et al (2013) Study of pore pressure change during mining and its application on water inrush prevention: a numerical simulation case in Zhaogezhuang coalmine, China. *Environ Earth Sci* 71(5):1–18

**Publisher’s Note** Springer Nature remains neutral with regard to jurisdictional claims in published maps and institutional affiliations.